Tutorial 8: Modern particle detectors

Dr. M Flowerdew

February 3, 2016

1 Introduction

In this tutorial, we will briefly review the techniques that are most commonly used for particle detection and energy/momentum measurements in modern high-energy physics collider experiments, such at those at LEP, the Tevatron and the LHC. A detector such as ATLAS (see Figure 1) consists of a large number of sub-detectors, each optimised for making a particular kind of measurement. Broadly speaking, these sub-detectors are arranged as follows:

- Tracking detectors, for measuring charged particles, closest to the interaction region.
- Calorimeters, for measuring electrons, photons and hadronic jets, surrounding the tracker.
- Muon detectors surrounding the calorimeters.

The ATLAS detector is used throughout as an example, where one is required. In addition to this, certain experiments will have specialised sub-detectors for other purposes, for example measuring the integrated luminosity, or performing detailed particle identification such as $\pi^{\pm}/K^{\pm}$ separation. These involve many extensions of the techniques described here, for example to simultaneously measure a particle's momentum and speed to obtain its mass. For brevity, we will neglect these more specialised topics, and focus on general-purpose detector design.

2 Tracking detectors

The purpose of a tracking detector, whether it is close to the interaction region or part of a muon detector, is to measure the trajectories of charged particles as precisely as possible, with minimal disturbance to their flight. They are almost invariably located within a magnetic field, so that the particles' momenta can be inferred from the radius of curvature.

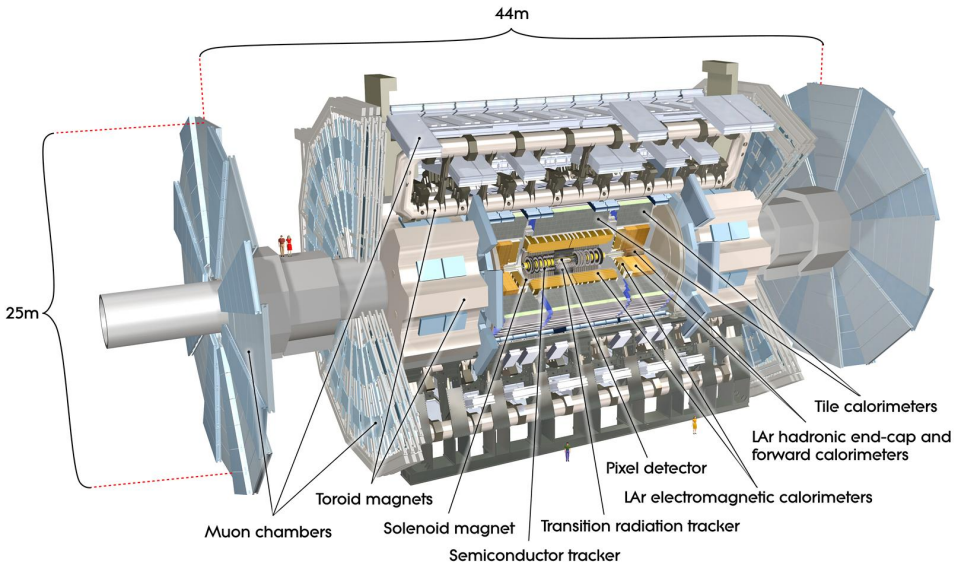

Figure 1: Cut-away view of the ATLAS detector.

Most often, the presence of a charged particle is detected by the ionisation it causes when passing through matter. This energy loss is desecribed by the Bethe-Bloch equation for a particle of charge q and speed βc:

$$\frac{\mathrm{d}E}{\mathrm{d}x} = -0.31 \frac{Z}{A} \rho \frac{q^2}{\beta^2} \left[\ln \left(\frac{2 m_e c^2 \beta^2 \gamma^2}{I} \right) - \beta^2 - \frac{\delta}{2} \right] \text{ MeV cm}^{-1}, \qquad (1)$$

where Z and A are the atomic and mass numbers of the material, respectively, ρ is its density, I the ionisation potential (typically $\sim 10Z$ if Z is large) and δ is a dielectric screening correction that is important when $\gamma \gg 1$.

The energy loss from ionisation and other sources for a muon passing through copper is shown as a function of $\beta\gamma$ in Figure 2. Although the details, including the magnitude of the energy loss, depend on the particle and material, the qualitative features of the curve as a function of $\beta\gamma$ are similar for most particles and most materials. There is a large region in particular, for $1 \lesssim \beta\gamma \lesssim 1000$, where the energy loss is small — for muons in copper this corresponds to momenta of around 0.1–100 GeV. Particles in this "minimum ionising" range will liberate enough electric charge to be detected, but will not be stopped by the material.

> **Exercise 1:** Estimate the thickness of copper that would be required to stop a muon with $p = 100$ GeV, using Figure 2. Only an order-of-magnitude estimate is required, but clearly state any simplifying assumptions you make.

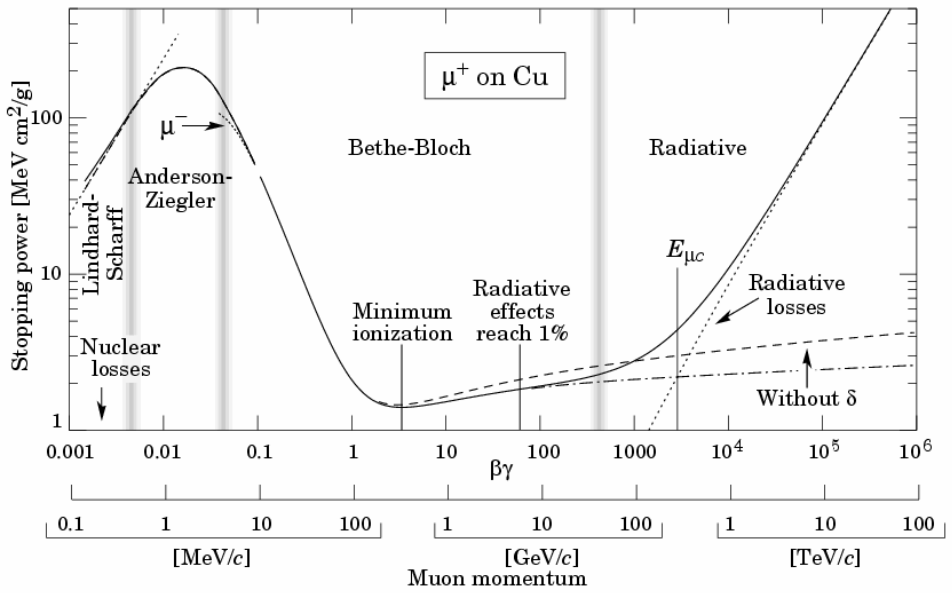

Figure 2: Illustration of the energy loss of muons in copper, as a function of $\beta\gamma$ of the muon and its momentum.

There are many different ways to build a tracking detector, although many share similar design principles. We will now discuss two of the most commonly used technologies — drift tubes and silicon.

2.1 Drift tube detectors

Many tracking detectors are made from arrays of *drift tubes*, such as the one illustrated in Figure 3. The wire located in the centre of the tube is held at a positive voltage relative to the tube wall, so that electrons liberated through ionisation will drift towards it with an average speed proportional

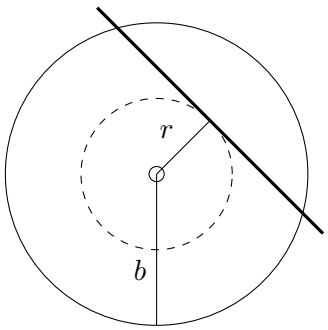

Figure 3: Cross-section of a drift tube, where a charged particle is passing through with an impact parameter of r.

to the local electric field, while ions migrate (more slowly) towards the wall. The electric field strength at a radius of r is proportional to $1/r$, increasing rapidly close to the wire. This allows the tube to exhibit several behaviours, depending on the wire radius a and the applied voltage V, as illustrated in Figure 4. Drift tubes for use in tracking detectors are generally operated within the proportional regime.

> **Exercise 2:** Describe the key qualitative features and physical origins of the detector response[a] in the ionisation, proportional and Geiger-Müller regions marked in Figure 4.

[a] A given detector may measure either current or voltage at the wire. Here, we will use the words "signal" and "response" as a generic term for either quantity.

Once the pulse has finished, *recombination* occurs and the tube becomes ready to accept a new signal. This process may emit UV photons, which can themselves cause ionisation and another cascade. A *quencher* is therefore usually required to stop the tube perpetually discharging. Polyatomic molecules such as CO_2, hydrocarbons or alcohols are good quenching materials, as they can absorb UV photons without being ionised.

> **Exercise 3:** How might a quencher molecule absorb a photon without being ionised or immediately re-radiating it? *Hint:* Where else might the absorbed energy go?

The choice of gas in a drift tube is dictated by a number of factors. Noble gases have few non-ionising modes for energy loss, and therefore support avalanches at low applied voltages. Many (e.g. Ar, Xe, Kr) are massive and thus yield many ion/electron pairs per unit path length (called *specific ionisation*). However, argon emits 11.6 eV photons during recombination, which can lead to permanent discharge unless appropriately quenched. Polyatomic gases can be self-quenching, however they must be circulated in order to remove free radicals that might damage the detector.

The measurement of a signal in a drift tube does not indicate an absolute position. Instead, the radius of closest approach r is deduced from the time (called t_0) between when the particle traversed the tube and when electrons first arrive at the wire.[1] Modern drift tube detectors typically have a time resolution of a few ns. With drift velocities typically of around 50 mm μs^{-1}, spatial resolutions of the order of $\delta r \sim 100$ μm can be achieved.

> **Exercise 4:** What effects, other than the electron drift time, need to be accounted for in the measurement of t_0? *Hint:* Think about the complete sequence of processes involved, from the initial particle

[1] More precisely, t_0 is determined by when the wire signal first passes some predefined threshold.

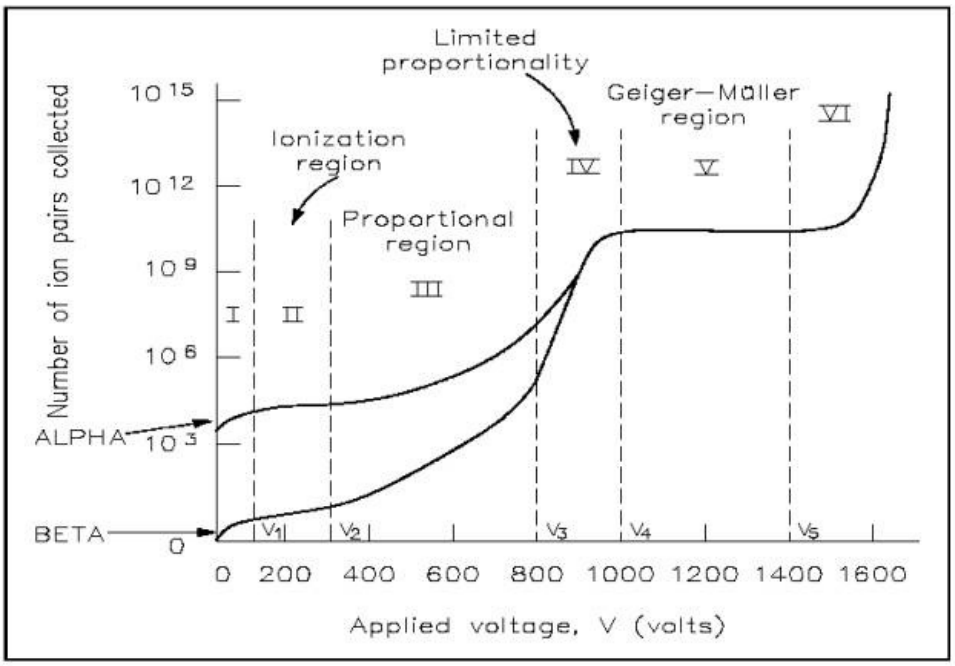

Figure 4: Response of a drift tube as a function of the applied voltage.

collision to the arrival of the signal at the on-detector electronics.

In real detectors, drift tubes are stacked, so that a single charged particle crosses multiple layers. This allows ambiguities in the drift circle measurement to be resolved, as the true particle track should pass tangentially to each measured drift circle. The tubes are ideally aligned along magnetic field lines, so that the curvature of the trajectory can be measured.

Exercise 5: While very precise, drift tube measurements have several shortcomings. For example, they only measure the drift-circle radius, not the position along the tube. Also, t_0 cannot be uniquely determined if the maximum possible drift time is much larger than the time between consecutive collisions.[a] How might these problems be overcome in a real-life detector?

[a] In ATLAS, the maximum drift time in the muon detector's drift tubes is several hundred nanoseconds, while collisions occur every 25 ns.

2.2 Silicon detectors

While relatively cheap and easy to make, drift tubes do not have sufficient resolution to distinguish hits from different particles very close to a collider's interaction region. In this region, semiconductor detectors are used, usually made using silicon. A cross-section of a silicon "strip" detector is shown in Figure 5. The sensor is essentially a collection of reverse-biased

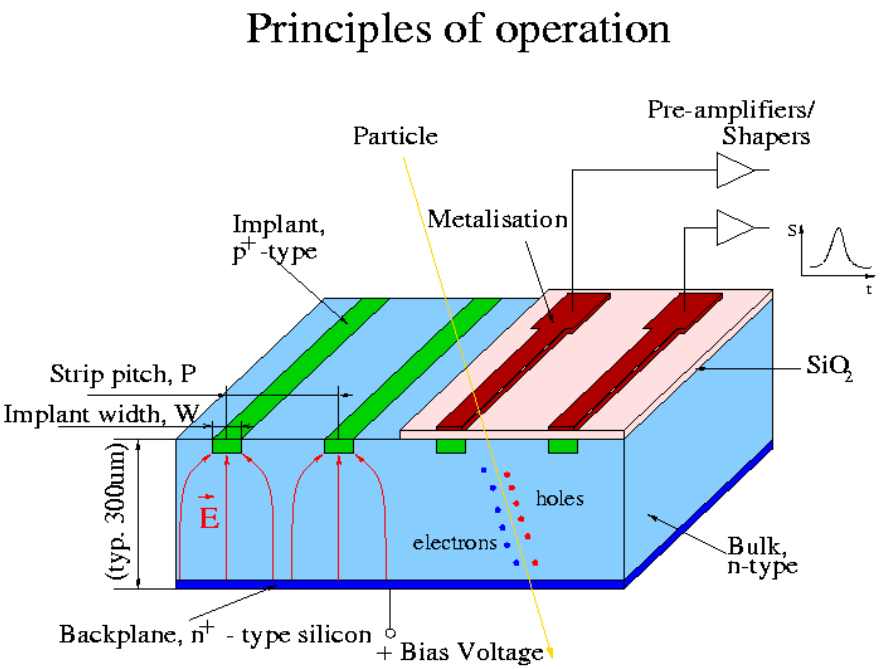

Figure 5: Schematic diagram of a p-in-n silicon strip detector. In a typical detector, the strip pitch would be of the order of μm, and the sensor thickness would be a few hundred μm. Individual strips can be several cm long.

diodes. In undoped silicon at room temperature and pressure, electrons in the conduction band and holes in the valence band result in $\mathcal{O}(10^{10})$ charge carriers per cubic centimetre. This is to be compared with about 100 pairs liberated per μm path length by a minimum ionising particle. Constructing a diode by combining p- and n-doped silicon creates a depletion zone at the join, with no free carriers. Applying a reverse-baised voltage causes the entire volume to be depleted, while simultaneously producing an electric field within the sensor, allowing efficient collection of the ionisation charge. Cooling the detector, for example with liquid nitrogen, also reduces the charge carrier density and the resulting leakage current. With modules typically a few hundred micrometres thick, many thousand electron/hole pairs can be formed, creating a clear signal even without further amplification.

In ATLAS, an extensive semiconductor tracker operating along these lines is used to reconstruct charged particle trajectories with a resolution of ~ 17 μm in the direction perpendicular to the strips. Modules are arranged in back-to-back pairs, with strips aligned with a small angle (40 μm) between them, to allow measurement of the hit position along the strip. The measurement in this direction is relatively coarse, with a resolution of

~ 580 μm. The strips are aligned along the magnetic field direction to give the best possible momentum resolution.

> **Exercise 6:** Consider a naive silicon detector design, where the strips of back-to-back modules are mutually perpendicular. In this design, the position resolution would depend less on the direction being measured. Try to think of reasons why this design is not used in ATLAS. *Hint:* Recall that the modules are several centimetres across, and that the particle density is very high close to the interaction point.

At radii of less than 250 mm, an even more precise tracking technology is used. Still based on silicon, a *pixel* detector has full two-dimensional granularity on a single chip, with pixel elements of dimension 50 μm$\times$400 μm in ATLAS. These give improved hit resolution of about 10 μm$\times$100 μm. Using pixels, rather than strips, not only improves the spatial resolution with less material (as back-to-back modules are not necessary), but they are also intrinsically more radiation-tolerant, suffer from lower noise levels and have fewer hit ambiguities. They are, however, significantly more complex and expensive to make.

One issue with silicon detectors, especially at the LHC, is that they degrade over time. Radiation damage can lead to vacancies and other lattice defects that decrease the charge carrier mobility and create new interstitial energy levels within the band gap. These interstitial levels allow charge carriers through the otherwise depleted material, increasing the leakage current, and hence the power consumption.

Over time, type-inversion can also occur, meaning that the n-type bulk becomes more like p-type silicon. This effect can be temporarily offset by increasing the applied bias voltage, again at the cost of greater leakage currents. The bias voltage cannot be increased indefinitely however, as eventually the risk of discharge (i.e. sparking) will become too great.

2.3 Momentum resolution

In order to measure the momentum of a charged particle, several measurements from drift tube and/or semiconductor tracking detectors must be combined. Figure 6 shows a sketch of a charged particle trajectory projected into the x–y plane, and the associated detector measurements. For this example, a magnetic field of magnitude B is aligned perpendicular to the diagram. In the absence of scattering effects (see later), the particle therefore follows a helical path. Momentum in the x–y, or *transverse*, plane is conventionally written as p_{T}. If the particle's electric charge is q, then the radius of curvature is

$$r = \frac{p_{\mathrm{T}}}{qB}. \tag{2}$$

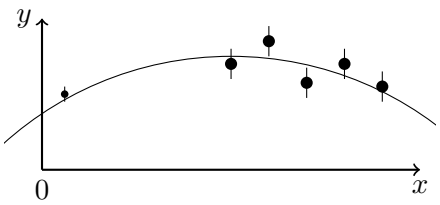

Figure 6: Sketch of a curved path fit, with contributions from one precision detector at $x \sim 0$ and five other measurements at higher x.

If the track is sufficiently straight, then the radius of curvature can be estimated by measuring the sagitta of the curve, defined in this case as the difference in y between the highest and lowest points of the curve.

Exercise 7: Suppose that the distance between the first and last detector elements in Figure 6 is L. Assuming that $r \gg L$, show first that the total angular deflection of the particle within the tracker can be written as $\Delta\phi = L/r$. Then, still using small-angle approximations, use this result to show that the sagitta s is

$$s = \frac{qBL^2}{8p_{\mathrm{T}}}. \tag{3}$$

Note that p_{T} can be expressed in terms of s and known quantities, if it is assumed that $|q| = 1$.

The resolution with which s can be determined, σ_s, depends on the number of x–y measurements and their intrinsic resolution. If the y measurements all have the same resolution σ_y, then σ_s will be proportional to σ_y, with a constant of proportionality depending on the geometry of the detector and the number of measurements. As s is proportional to $1/p_{\mathrm{T}}$, we then find that

$$\frac{\sigma_{p_{\mathrm{T}}}}{p_{\mathrm{T}}} = \frac{\sigma_s}{s} \propto \frac{\sigma_y p_{\mathrm{T}}}{BL^2}. \tag{4}$$

This suggests the following design principles to obtain precise momentum measurements for particles with large p_{T}:

- a strong magnetic field B;
- a physically large detector (large L);
- good intrinsic detector resolution σ_y;
- many detector layers (not shown in Equation (4)).

The other main factor affecting the momentum resolution of a tracking detector is *multiple scattering*. This, illustrated in Figure 7, describes the

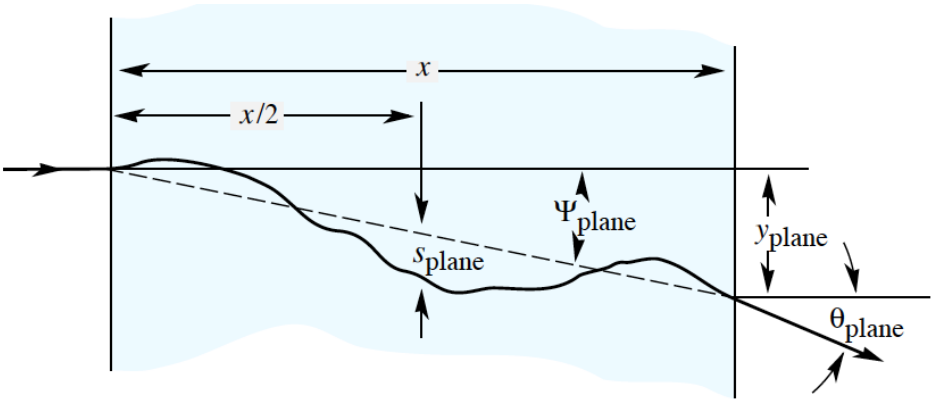

Figure 7: Illustration of multiple scattering of a particle (incident from the left) in material.

changes in position and direction (also energy loss) that a charged particle undergoes as it traverses material. Upon passing a distance x through a material, a particle will emerge with a displacement y_{plane} and angle θ_{plane} relative to its original trajectory.[2] In the absence of large-angle scattering, these can be described by Gaussian probability distributions with the following width parameters:

$$y_{\text{plane}}^{\text{rms}} = \frac{1}{\sqrt{3}} x\theta_{\text{plane}}^{\text{rms}} = \frac{1}{\sqrt{3}} x\theta_0,$$
$$\text{where } \theta_0 = \frac{13.6 \text{ MeV}}{\beta cp}\sqrt{\frac{x}{X_0}}\left[1 + 0.038 \ln\left(\frac{x}{X_0}\right)\right]. \tag{5}$$

Here, X_0 is the *radiation length*, a property of the material which will be further described in the section on calorimetery (see especially Equation (8)), and a unit charge for the incident particle is assumed. Multiple scattering represents a fundamental limit on the position and angular resolution of a given detector.

Exercise 8: Show that the contribution of multiple scattering to the transverse momentum resolution has the following dependence on B, L and p_{T}:

$$\frac{\sigma_{p_{\text{T}}}}{p_{\text{T}}} \propto \frac{1}{B\sqrt{L}}. \tag{6}$$

Hint: First write $\Delta\phi$ in terms of p_{T}, and use this to relate the momentum resolution from multiple scattering to the resolution of $\Delta\phi$. You

[2] In both cases, "plane" indicates that we are using a 2D projection. When the RMS deviations are considered, the corresponding values in 3D space are a factor of $\sqrt{2}$ larger than those quoted.

may neglect the $\ln(x/X_0)$ term from Equation (5).

Exercise 9: Consider a relativistic muon passing through 1 m of magnetised iron ($B = 2$ T, perpendicular to p. $X_0^{\mathrm{Fe}} = 1.8$ cm). If the muon's direction of travel is measured before and after it traverses the iron, what is the best fractional momentum resolution that can be expected, based on multiple scattering effects alone?

Combining Equations (4) and (6), we can write the total p_{T} resolution in the following way:

$$\frac{\sigma_{p_{\mathrm{T}}}}{p_{\mathrm{T}}} = Ap_{\mathrm{T}} \oplus B. \tag{7}$$

The first term arises from the intrinsic measurement resolution of the detector elements, while the second arises from multiple scattering, and the $\oplus$ indicates addition in quadrature. This expression allows us to see by inspection that the main contribution to the measurement resolution depends on p_{T}. Multiple scattering is most important when p_{T} is small, while the intrinsic detector properties become more important as the p_{T} increases.

3 Calorimetry

The purpose of a calorimeter is to measure the energy of incoming particles by completely absorbing them. Coupled with a measurement of the direction of motion, this allows the 3D momentum of relativistic particles to be reconstructed. In contrast with tracking detectors, calorimeters can detect both charged and neutral particles, through a number of different processes. Modern high-energy experiments take advantage of this, with separate subdetectors optimised for electromagnetic and hadronic interactions.

3.1 Electromagnetic calorimetry

In Figure 2, it can be seen that extremely relativistic particles ($\beta\gamma \gtrsim 1000$) lose energy mainly through radiation.[3] For currently accessible energies, this is only relevant for the electron.[4] The critical energy, E_c, for electrons, where radiative losses are greater than ionisation losses, is approximately 0.6 GeV/Z, where Z is the atomic number of the material.

The radiation of a photon by an electron in a material is illustrated in Figure 8a. The electron can interact coherently with an entire nucleus, giving a contribution $Z\sqrt{\alpha}$ to the amplitude. The cross section for this process is therefore proportional to $Z^2\alpha^3$. The electron can also scatter from atomic electrons, but as this is not coherent the contribution is much

[3] Recall that, while Figure 2 refers specifically to muons, the qualitative features are valid for all particles, if only EM interactions are considered.

[4] and, of course, the positron.

Element	X_0 [cm]	λ [cm]
air	30,400	75,000
graphite	18.8	38.1
Al	8.9	39.4
Fe	1.8	16.8
Pb	0.6	17.1

Table 1: Radiation and interaction lengths for five example materials at a temperature of 20°C and 1 atm pressure.

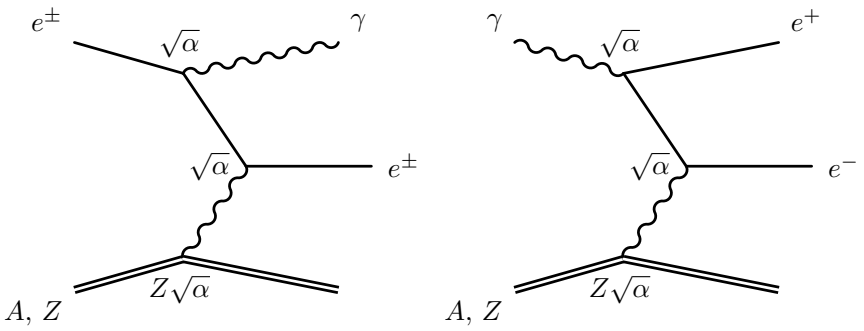

(a) Bremsstrahlung (b) Photon conversion

Figure 8: Diagrams for electron and photon interactions in matter.

smaller, proportional to $Z\alpha^3$. The electron loses energy exponentially, with a rate parameterised by the *radiation length* X_0:

$$\frac{\mathrm{d}E}{\mathrm{d}x} = -\frac{E}{X_0},$$

$$\text{where } \frac{1}{X_0\,[\mathrm{cm}]} \approx 4\left(\frac{\hbar}{mc}\right)^2 Z(Z+1)\alpha^3 n_A \ln\left(\frac{184}{Z^{1/3}}\right). \tag{8}$$

Here, n_A is the number density in cm^{-3}. Note that X_0 is often quoted in $\mathrm{g{\cdot}cm}^{-2}$, which is related to this definition by the density ρ. The radiation length depends strongly on the material involved, decreasing rapidly for denser elements. Radiation lengths for some common materials are given in Table 1. The radiation lengths of most solid materials are of the order of centimetres.

High energy photons interact with matter in a similar way to electrons, creating electron-positron pairs (see Figure 8b). This is related to the diagram in Figure 8a by an exchange of ingoing and outgoing particles. The cross section is therefore similar, and the characteristic length for this process is $\frac{9}{7}X_0$.

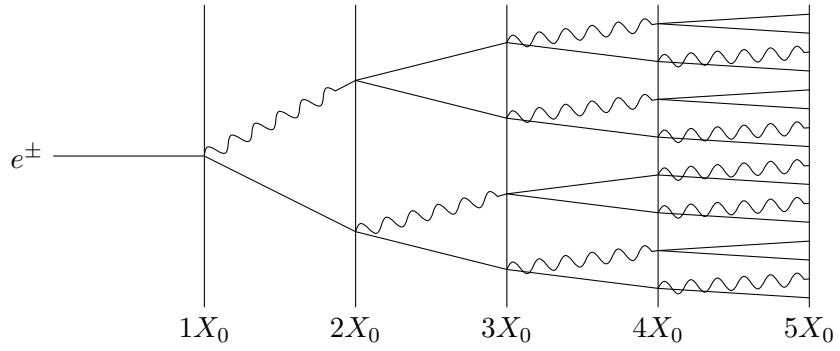

Figure 9: The Rossi model of an electromagnetic calorimeter shower.

Combining these two processes allows us to build up a simple picture of what happens when a high-energy electron (or, with minor modifications, a photon) enters a dense material. After a distance $\mathcal{O}(X_0)$, it will undergo Bremsstrahlung, producing a high-energy photon. The electron (after interaction) and the photon can be expected to have comparable energies. They will both propagate more or less freely for a further distance $\mathcal{O}(X_0)$, with the electron only losing a small fraction of its energy to ionisation of the material. Then, the electron will undergo Bremsstrahlung again, and the photon will convert into an e^+e^- pair. Again, it is reasonable to assume that all four particles (two electrons, one positron and one photon) will have comparable energies, and they will each travel a distance $\sim X_0$ before undergoing further significant interactions. This process will continue until the particles have energies below the critical energy for Bremsstrahlung, at which point all of the charged particles will lose their remaining energy through ionisation. This simple model of an *electromagnetic (EM) shower* is illustrated in Figure 9.

This model is highly simplified, and yet it illustrates certain key features of EM showers very well. Consider the shower at the n^{th} step, i.e. at a distance of nX_0 into the material. At this step, there will be 2^n particles in the shower, each with an energy of $E_n = E_0/2^n$ (if the original incident particle had an energy E_0). The shower ends at some step N when E_N equals the critical energy E_c.

Exercise 10: Solve for N and show that the total shower depth increases logarithmically with E_0. This is a very important property of EM (and hadronic) showers, as it means that detector sizes do not have to scale proportionally to collider energies.

Exercise 11: If N is large, show that the total number of particles in the shower is proportional to E_0. Does this result hold separately for

the number of photons and $e^{\pm}$, or only for the sum?

Although we will not prove it, the shower width is also proportional to X_0. For example, a shower of depth $20X_0$ will have a width of approximately by $(21.2 \text{ MeV}/E_c)X_0$.

Lead tungstate ($PbWO_4$) is a common EM calorimeter material. It has a high density and constituent atoms with high atomic numbers, and therefore a short radiation length of just 0.89 cm. In addition, it scintillates and is itself transparent to the light produced, allowing this to be collected by a photodiode or similar photodetector. However, it is brittle and can be difficult to work with. Another approach is to separate the tasks of producing and detecting the shower by interleaving layers of a dense *absorber* (such as lead or steel) with ionisation or scintillation detectors. This design is referred to as a *sampling calorimeter*, because the shower is sampled at intervals as it evolves. The EM calorimeter in ATLAS uses this latter approach, with liquid argon (LAr) being used as the ionisation medium, while CMS has an EM calorimeter based on lead tungstate.

The proportionality between the energy and the number of shower particles is only true on average. If a particle of energy E would produce ν charged particles on average, the number observed in any particular shower will be described by Poisson statistics:

$$P(n_{\text{obs}}) = e^{-\nu}\frac{\nu^{n_{\text{obs}}}}{n_{\text{obs}}!}. \tag{9}$$

This distribution has the property that both the mean and the variance of n_{obs} are equal to ν. Variations in the energy measured will vary as $\delta(n_{\text{obs}}) = \sqrt{\text{var}(x)} = \sqrt{\nu}$. As ν is proportional to the particle's energy, the statistical uncertainty on the energy measured will vary as $\sqrt{E}$. Equivalently, the fractional resolution σ_E/E varies as $1/\sqrt{E}$, improving as E increases.

The total energy resolution for most calorimeters can be written in the following way:

$$\frac{\sigma_E}{E} = \frac{A}{\sqrt{E}} \oplus B \oplus \frac{C}{E}. \tag{10}$$

The first term is the stochastic term just discussed. The second, constant, term arises from inhomogeneities in the calorimeter response and its calibration. The final term arises from electronic noise, and can be important for low energy particles. For the ATLAS EM calorimeter, $A = 10\%$ if E is in GeV, and $B = 0.7\%$. As before, these numbers are added in quadrature to obtain the total resolution function.

3.2 Hadronic calorimetry

Due to their higher mass,[5] high-energy hadrons do not lose significant amounts of energy through electromagnetic processes (see again Figure 2). Their

[5]The lightest hadron, the pion, has a mass similar to that of the muon.

hadronic interactions consist of three components:

- elastic scattering from nuclei;
- quasi-elastic scattering, i.e. elastic scattering from nucleons;
- inelastic scattering.

The last two of these are responsible for producing a *hadronic shower*, with each inelastic scatter producing more hadrons that may each then undergo an inelastic collision, and so on. As with an EM calorimeter, measuring the energy of the original hadron then reduces to counting the total number of particles produced in this way.

The hadron-nucleus inelastic cross section scales with the nuclear cross-sectional area:

$$\sigma_{\text{inel}} \approx \sigma_{pp} A^{\frac{2}{3}}. \tag{11}$$

The proton-proton inelastic cross section σ_{pp} is about 30 mb, much smaller than for EM interactions. Therefore, the so-called *interaction length* λ is much longer than the EM equivalent X_0. The interaction length is defined as

$$\lambda = \frac{1}{n\sigma_{\text{inel}}}, \tag{12}$$

where n is the number density of the material. Typical values for some materials are shown in Table 1.

With interaction lengths of tens of centimetres, even a calorimeter made out of lead or steel will need to be very large in order to guarantee the capture of an entire hadronic shower - typically a depth of 20λ would be required. Due to the resulting size requirements, most hadronic calorimeters are of the sampling variety, with very dense, high-A absorbers. Scintillators are often used to measure the shower, where several scintillating sheets can be connected to a single photomultiplier tube via optical fibres. Such an arrangement can be seen in Figure 10. Other possibilities include collecting charge on electrode plates on either side of an ionising medium, or inserting small multi-wire proportional chambers between the absorber layers.

The resolution of a hadronic calorimeter is described in the same way as that of an EM calorimeter (Equation (10)), however the absolute values of the coefficients are usually much larger. This is due partly to the large interaction lengths involved and the greater probability of lateral or longitudinal shower leakage, but also due to the energy lost in elastic scattering, which does not increase the number of particles in the shower. In the ATLAS hadronic calorimeter, $A = 50\%$ and $B = 3\%$.

One other factor affecting the hadronic energy resolution is that there may be EM showers contained within the hadronic shower, for example from $\pi^0 \to \gamma\gamma$ decays. The response of most calorimeters to these EM components is substantially different to the hadronic component, and the EM energy

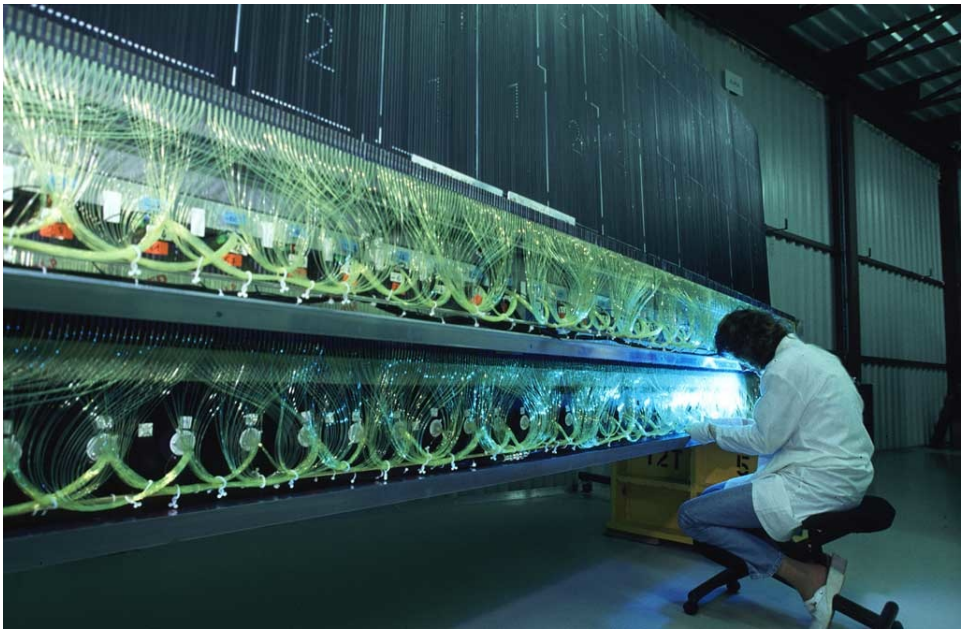

Figure 10: Part of the ATLAS hadronic calorimeter during construction.

fraction is a significant source of uncertainty in the energy measurement. Usually, the response to EM showers is greater, due to the nuclear binding energy in hadronic interactions, losses from neutrinos in hadron decays, and other effects. It is possible to tune the calorimeter design to offset these effects, for example by:

- increasing the absorber thickness (which suppresses detection of EM showers);
- using a radioactive absorber, which can undergo fission in the presence of slow neutrons, increasing the overall response to hadrons;
- using light nuclei in the absorber, which can also give sensitivity to slow neutrons.

This kind of design is called a *compensating calorimeter*. A recent example of this kind of design is the ZEUS calorimeter, which used depleted uranium to increase the hadronic response. Its stochastic resolution term was indeed good, at $A = 35\%$ (compared with 50% for ATLAS). This comes with a cost however: ZEUS' stochastic term coefficient for EM showers was 18%, compared to 10% for ATLAS. The different design choices in this case reflect the different experimental goals in the two cases: precision QCD measurements in the case of ZEUS, versus Higgs boson and other TeV-scale discoveries in the case of ATLAS.